CHAPTER 2

CONSTANT TORQUE LIMIT CONTROL STRATEGY FOR SMPMSM DRIVES

2.1 Introduction

Due to the merits of being able to achieve high efficiency, higher torque to inertia ratio, high power density and free from maintenance, surface mounted permanent magnet synchronous motors (SMPMSM) have now been widely adopted for servo drives in various applications.

To achieve both fast dynamic response and high performance for four quadrant operation, a vector control is usually used in the SMPMSM drives. When the synchronous rotating d-axis is in alignment with the direction of the north pole of the rotor permanent magnet, the d-axis and q-axis currents corresponds to the d-axis flux and torque component, respectively. Due to the non-salient property, the developed torque depends only on q-axis current. Therefore, one can take advantage of this degree of freedom to control the d-axis current to achieve some predefined performance index. There are some different torque control strategies [3], such as zero d-axis current (maximum torque per ampere), maximum efficiency, unity power factor and constant mutual flux linkages, when the operating speed is lower than base speed. However, the zero d-axis current is the most popular method used in industrial applications [3]. Although the d-axis current is usually chosen to be zero to get the merit of easy implementation and to achieve maximum torque per ampere control, the required stator voltage may exceed the capacity of the inverter when the rotor speed exceeds some rated value [4]. Thus, to take fully advantage of the capability of the drives, the constraints of the SMPMSM drives is required for the design of the

controller.

The rest of this chapter is outlined as follows. In section 2.2, the mathematical model and constraints of the SMPMSM drives are first reviewed briefly. Then, the classification of operation regions for four-quadrant operation is presented in section 2.3. Also, the profound effects resulted from the consideration of the stator resistance is clarified therein. Finally, some constant torque limit control strategies for PMSM drives operated for lower than base speed are discussed briefly and some experimental results resulting from a DSP-based prototype drive are given to verify the validity and limit of the torque control strategy in which the d-axis current is kept zero. Additionally, some experiments are conducted to demonstrate the classification of ten regions for four quadrant operation and to verify the effects of stator resistance.

2.2 Mathematical Model and Constraints of SMPMSM Drives

Fig. 2.1 shows the cross section of a 4-pole and 24-slot SMPMSM [62]. The mathematical model of the SMPMSM drive system in the synchronous reference frame can be described as follows [58].

$$v_{ds} = R_s i_{ds} + \frac{d}{dt}\lambda_{ds} - \frac{p}{2}\omega_r \lambda_{qs} \quad (2.1)$$

$$v_{qs} = R_s i_{qs} + \frac{d}{dt}\lambda_{qs} + \frac{p}{2}\omega_r \lambda_{ds} \quad (2.2)$$

$$\lambda_{ds} = L_s i_{ds} + \lambda_f \quad (2.3)$$

$$\lambda_{qs} = L_s i_{qs} \quad (2.4)$$

$$T_e = (3/2)(p/2)\lambda_f i_{qs} \quad (2.5)$$

where v_{ds}, v_{qs}: stator d-axis, q-axis voltages

$\omega_e \equiv \frac{p}{2}\omega_r$: rotor electrical angular speed

i_{ds}, i_{qs} : stator d-axis, q-axis currents

R_s : stator resistance

L_s : stator inductance

$\lambda_{ds}, \lambda_{qs}$: stator d-axis, q-axis flux linkages

λ_f : flux linkage due to the permanent magnet

ω_r : rotor mechanical angular speed

p : number of poles

T_e : electromagnetic torque.

From (2.1) and (2.2), one can obtain the following steady state equations

$$v_{ds} = R_s i_{ds} - \omega_e L_s i_{qs} \tag{2.6}$$

$$v_{qs} = R_s i_{qs} + \omega_e (L_s i_{ds} + \lambda_f) \tag{2.7}$$

Also, for a fixed inverter capacity, one can include the following inequality constraints

$$i_{ds}^{\ 2} + i_{qs}^{\ 2} \le I_{sm}^{\ 2} \tag{2.8}$$

$$v_{ds}^{\ 2} + v_{qs}^{\ 2} \le V_{sm}^{\ 2} \tag{2.9}$$

where V_{sm} is the maximum phase voltage magnitude and I_{sm} is the maximum phase current magnitude.

By substituting (2.6) and (2.7) into (2.9), one can get the following voltage constraint in terms of the stator current variables:

$$(i_{ds}+\frac{\omega_e{}^2 L_s \lambda_f}{R_s{}^2+\omega_e{}^2 L_s{}^2})^2+(i_{qs}+\frac{\omega_e R_s \lambda_f}{R_s{}^2+\omega_e{}^2 L_s{}^2})^2 \le \frac{V_{sm}{}^2}{R_s{}^2+\omega_e{}^2 L_s{}^2} \tag{2.10}$$

The above voltage constraint depends not only on the parameters of the SMPMSM, namely R_s, L_s, λ_f and V_{sm}, but also on the rotor speed ω_r ($\omega_r = \frac{2}{p}\omega_e$).

2.3 Classification of Operation Regions for four-quadrant operation

To achieve fast response, it is essential to apply the maximum available torque to the drive system. Conventionally, the operation region is divided into the constant torque limit control region and the field weakening control region. However, as will be explained later, there exists a partial field weakening control region where either a zero i_{ds} control or a field weakening control should be applied depending on the load torque magnitude. For easy explanation, only the first and the fourth quadrant operation modes, for positive speed portion, on the conventional torque vs. speed plane will be given. The remaining two quadrant operation modes, namely for the negative speed portion, are explained later. For easy understanding, a SMPMSM, whose parameters are shown in Table 2.1, where V_{sm} =50 V and I_{sm} =2 A are used as an example to illustrate its five operation regions for positive speed operation. Fig.2.2 (a) shows the circular current limit constraint and five voltage constraints corresponding to five positive speeds, namely ω_{rm}, ω_{r1}, ω_{rc}, ω_{rn} and ω_{re} in the increasing order respectively. Since the corresponding voltage limits for negative speeds are symmetric to i_{ds} axis, only those voltage constraints for positive speeds are shown in Fig. 2.2(a). On the contrary, Fig. 2.2(b) shows the one for the negative speeds.

Region 1: $0 \le \omega_r \le \omega_{rm}$, $0 < T_e \le T_{eM1}$

This region is called the forward constant torque limit region. The available maximum torque in this region, called forward constant torque limit, is given as follows

$$T_{eM1} = \frac{3}{2}\frac{p}{2}\lambda_f I_{sm} \tag{2.11}$$

TABLE 2.1. THE PARAMETERS OF THE TESTED SMPMSM

number of poles (p)	8	magnetic flux linkage (λ_f)	$0.0579(V/(rad/\sec))$
stator resistance (R_s)	$3.55\ \Omega$	rotor inertia	$6.45\times10^{-5} kg/m^2$
stator inductance (L_s)	$5.92\ mH$	viscous damping coefficient	$8\times10^{-5}(N\cdot m\cdot\sec/rad)$

By adopting the equality sign of (2.10) and letting (i_{ds}, i_{qs}) = $(0, I_{sm})$ one can obtain the limiting speed (ω_{rm}) of this region as follows

$$\omega_{rm} = \frac{2}{p}\frac{-2R_s I_{sm}\lambda_f + \sqrt{(2R_s I_{sm}\lambda_f)^2 - 4(\lambda_f{}^2 + L_s{}^2 I_{sm}{}^2)(R_s{}^2 I_{sm}{}^2 - V_{sm}{}^2)}}{2(\lambda_f{}^2 + L_s{}^2 I_{sm}{}^2)} \tag{2.12}$$

From Fig. 2.2(a) one can see that in this region, the actual i_{ds} and i_{qs} current command trajectory just corresponds to the line segment from point O to point A.

Region 2: $\omega_{rm} < \omega_r \le \omega_{rc}$, $0 < T_e \le T_{eM2}(\omega_r)$

This region is called the forward partial field weakening region. In this region it is seen that i_{ds} becomes negative to achieve field weakening control. However, as can be observed from Fig. 2.2(a) that if the drive speed is ω_{r1} then for a heavy load whose i_{qs} trajectory corresponds to line $H_1 - H_2 - H_3$, the allowed maximum torque

per ampere control should be located at point H_2 on the voltage constraint curve. The zero i_{ds} control at point H_3 is not feasible. However, in the case under light load condition as shown in Fig. 2.2(a), its feasible i_{qs} trajectory corresponds to line $L_1 - L_2 - L_3$. Obviously, the maximum torque per ampere control is now located at L_2 with zero i_{ds}. In summary, in this region there are two control modes which should be chosen according to the actual load torque requirement. Similarly, the boundary speed ω_{rc} can be obtained from (2.10) by letting (i_{ds}, i_{qs})=(0,0):

$$\omega_{rc} = \frac{2}{p}\frac{V_{sm}}{\lambda_f} \tag{2.13}$$

Also, the available maximum torque trajectory in this region varies with ω_r and the corresponding i_{ds}, i_{qs} trajectory is located on the ABC arc of Fig. 2.2(a). For each speed ω_r, one can use the current and voltage constraints to calculate the intersecting point $(i_{ds}(\omega_r), i_{qs}(\omega_r))$. Hence, with this calculated $i_{qs}(\omega_r)$ the corresponding available maximum torque $T_{eM2}(\omega_r)$ at ω_r can be obtained from (2.5).

Region 3: $\omega_{rc} < \omega_r \le \omega_{re}$, $0 < T_e \le T_{eM3}(\omega_r)$

This region is called the forward full field weakening region. Only negative i_{ds} current control is allowed in this region. Similarly, the available maximum torque $T_{eM3}(\omega_r)$ in this region varies with speed and can be obtained in a manner similar to that of region 2. The corresponding i_{ds}, i_{qs} trajectory is located on the CDE arc of Fig. 2.2(a) and the boundary speed ω_{re} can be determined from (2.10) by letting (i_{ds}, i_{qs})=$(-I_{sm}, 0)$:

$$\omega_{re} = \frac{2}{p}\sqrt{\frac{V_{sm}{}^2 - R_s{}^2 I_{sm}{}^2}{(\lambda_f - L_s I_{sm})^2}} \tag{2.14}$$

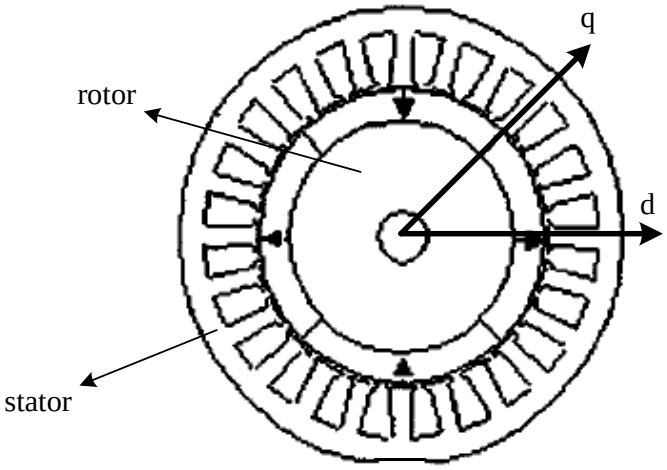

Fig. 2.1. The cross section of a 4-pole and 24-slot SMPMSM. [62]

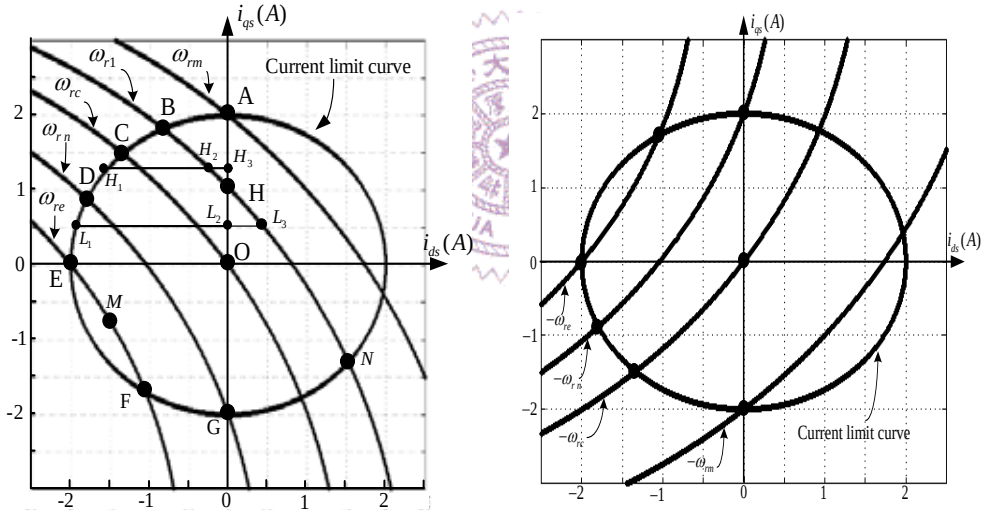

(a) (b)

Fig. 2.2. The trajectories of the current limit curve and five voltage limit curves for ω_r on $i_{ds}-i_{qs}$ plane for a SMPMSM. (a) for positive speed; (b) for negative speed.

Region 4: $0 < \omega_r \le \omega_{r\ n}$, $T_{eN1} \le T_e < 0$

This region is called the forward constant braking torque limit region. As can be observed from point G of Fig. 2.2(a), the available maximum braking torque is

$$T_{eN1} = -(\frac{3}{2}\frac{p}{2}\lambda_f I_{sm}) \tag{2.15}$$

The boundary speed $\omega_{r\,n}$ is given as

$$\omega_{r\,n} = \frac{2}{p}\frac{2R_s I_{sm}\lambda_f + \sqrt{(2R_s I_{sm}\lambda_f)^2 - 4(\lambda_f{}^2 + L_s{}^2 I_{sm}{}^2)(R_s{}^2 I_{sm}{}^2 - V_{sm}{}^2)}}{2(\lambda_f{}^2 + L_s{}^2 I_{sm}{}^2)} \tag{2.16}$$

Region 5 : $\omega_{r\ n} < \omega_r \le \omega_{re}$, $T_{eN2}(\omega_r) \le T_e < 0$

This region is called the forward weakening braking torque limit region. From Fig. 2.2(a) one can see that the corresponding i_{ds}, i_{qs} trajectory simply corresponds to the GF arc portion of the circular current limit. Obviously, the maximum braking torque $T_{eN2}(\omega_r)$ changes with the drive speed and can be obtained similar to the previous process.

The remaining two quadrant operation modes, namely for the negative speed portion, are symmetric to the previous ones as can be observed from the dependency on ω_e in (2.10). Therefore, the other five regions corresponding to negative speed portion can be classified in the ways similar to region 1 to 5. For convenience and consistency, the following symbols defined in region 6 to 10 are the same as the definitions defined in region 1 to 5.

Region 6: $-\omega_{rm} \le \omega_r \le 0$, $-T_{eM1} < T_e \le 0$

This region is called the backward constant torque limit region. The available

maximum torque in this region, called backward constant torque limit, is given as $-T_{eM1}$.

Region 7: $-\omega_{rc} < \omega_r \le -\omega_{rm}$, $-T_{eM2}(\omega_r) < T_e \le 0$

This region is called the backward partial field weakening region. In this region it is seen that i_{ds} becomes negative to achieve field weakening control. Similar to region 2, in this region there are two control modes which should be chosen according to the actual load torque requirement.

Region 8: $-\omega_{re} < \omega_r \le -\omega_{rc}$, $-T_{eM3}(\omega_r) < T_e \le 0$

This region is called the backward full field weakening region. Similar to region 3, only negative i_{ds} current control is allowed in this region.

Region 9: $-\omega_{r\ n} < \omega_r \le 0$, $0 \le T_e < -T_{eN1}$

This region is called the backward constant braking torque limit region. The maximum braking torque for backward operation is kept on $-T_{eN1}$, namely T_{eM1}.

Region 10 : $-\omega_{re} < \omega_r \le -\omega_{r\ n}$, $0 \le T_e < -T_{eN2}(\omega_r)$

This region is called the backward weakening braking torque limit region. And the maximum braking torque for backward operation will vary with the speed.

To give a better overall view about the five operation regions, Fig. 2.3(a) shows the available maximum torque limit trajectories for different operation modes. It is also interesting to see the effects of neglecting the small stator resistance R_s as adopted often in existing literature. Fig. 2.3(b) shows the corresponding trajectories for the same SMPMSM. Comparison of these two figures shows quite significant differences as follows:

. First, T_{eM2} and T_{eM3} are overestimated if R_s equals zero. Also, the partial field weakening region, both forward and backward portion, becomes narrower.

. Second, the maximum braking torques (namely T_{eN1} and T_{eN2}) are underestimated and will result in slower response during the braking period.

. Finally, the symmetric property of Fig. 2.3(b) is no longer true if R_s is considered.

In summary, for four quadrant operations, there are ten operation regions. Half of them belong to positive speed operation and the other half are for negative speed operation.

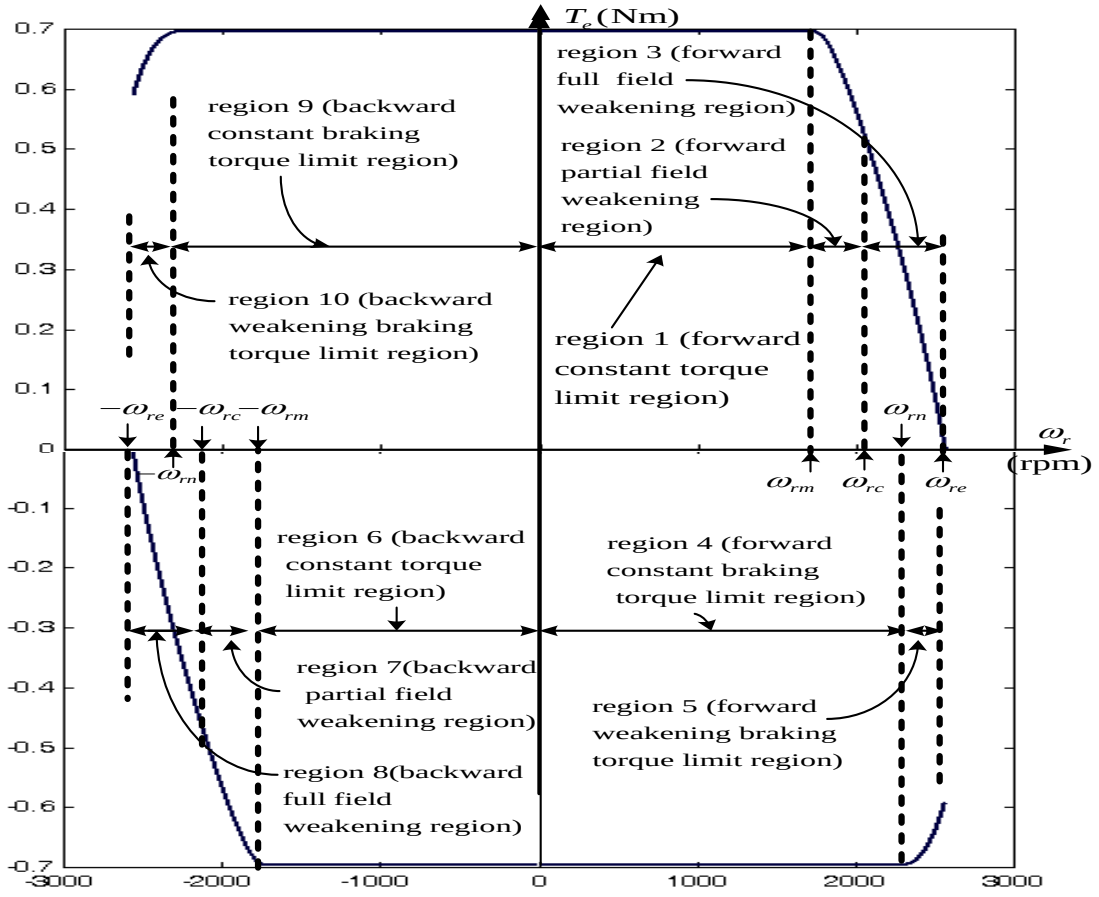

(a)

Fig. 2.3. Trajectories of the available maximum torques in different regions (a) without neglecting R_s; (b) neglecting R_s.

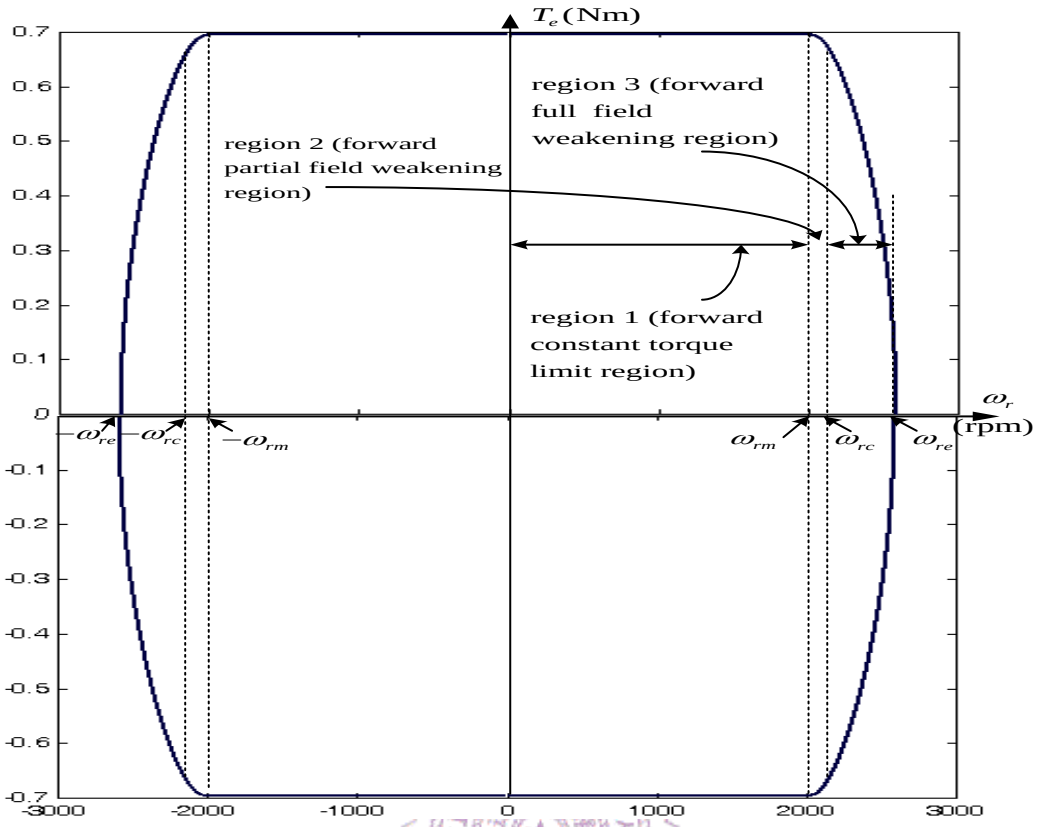

(b)

Fig. 2.3. Trajectories of the available maximum torques in different regions (a) without neglecting R_s; (b) neglecting R_s. (continued).

2.4 Constant Torque Limit Control Strategy and Experimental Results

In view of previous discussion, regions 1, 4, 6 and 9 can be considered as constant torque limit regions due to the magnitude of the available torque is keep constant, namely $\frac{3}{2}\frac{p}{2}\lambda_f I_{sm}$. The main existing torque control strategies for PMSM drives operated in above constant torque limit regions are as follows:

(a) Zero d-axis current

(b) Maximum efficiency

(c) Unity power factor

(d) Constant mutual flux linkages

The zero d-axis current control strategy is popular in industrial applications. The main benefits of this strategy are the simple implementation and the achievement of maximum ratio of torque per ampere. As a result, the minimum copper loss objective can also be obtained. However, the net loss of the zero d-axis current control strategy is not the global minimum value. On the contrary, the maximum efficiency control strategy minimizes the net loss of the PMSM drives at any operating condition, but the fast and exact control performance will be based on the exact information of the core loss [60]. However, this requirement is very difficult to meet in practice. The unity power factor control strategy minimizes the rating of the apparent power of the inverter by keeping the power factor to be unity [9]. The constant mutual flux linkages control strategy keeps the air gap flux to a constant value, and results in a seamless flux weakening strategy for the SMPM drives [9]. Although each of the above strategies has its own merits and demerits, the zero d-axis current control strategy [3] is still the most popular one at present. Hence, this control strategy is adopted for the constant torque limit control region in this dissertation.

To facilitate understanding and also as a verification of the characteristics explained in this chapter, a digital controller is constructed according to the block diagram of Fig.2.4. A digital signal processor, namely TMS320F240 is adopted for implementation. The same SMPMSM whose parameters are shown in Table 2.1 is chosen as the tested motor. For consistency, the dc link voltage and I_{sm} are chosen to be 100V and 2A, respectively. Due to the applying of sinusoidal pulse-width modulated (SPWM) inverter, the corresponding V_{sm} is 50 V. Thus, the corresponding ω_{rm}, ω_{rc} and $\omega_{r\ n}$ are found to be 1737, 2060 and 2298 rpm from equations (2.12), (2.13) and (2.16), respectively. The block diagram of the adopted

speed control system for the tested SMPMSM drive is shown in Fig 2.4. From Fig 2.4, one can see that except the PI speed controller with variable-bounds antiwindup, the upper/lower (U/L) I_{qs} bounds calculator and the minimum copper loss (MCL) controller, all other blocks are basically rather typical and no additional explanation is required. The detailed derivation and explanation of three major blocks will be given in the next chapter and only brief explanation is given in this section. The detailed description of implementation of hardware and software will be presented in chapter 3. A PI speed controller with variable-bounds antiwindup is adopted to eliminate the performance deterioration resulting from the saturation problems of the integrator, the PI speed controller adopted in this dissertation is shown in Fig. 2.5. However, the saturation bounds, $I_{qs\max}$ and $I_{qs\min}$, must correspond to the actual available maximum accelerating and decelerating torque ability, as shown in Fig 2.2. The upper/lower (U/L) I_{qs} bounds calculator compute the saturation bounds and fed to PI speed controller. Therefore, the saturation bounds will vary with the variation of rotor speed if the drive is operated on the field weakening regions, namely regions 2, 3, 5, 7, 8 and 10. According to the proposed concept of partial field weakening, one can choose a proper d-axis current command to achieve minimum copper loss operation for a MCL controller. The sampling time period for the PI speed controller with constant-bounds antiwindup is chosen to be 1.0 ms. In contrast, the sampling time period of the current controller is chosen as 0.1 ms.

Several experimental results are provided below to show the characteristics explained in this chapter. First, to demonstrate the starting performance Fig.2.6 shows the responses of speed command (ω_r^*), speed (ω_r), d-axis current command (i_{ds}^*), d axis current (i_{ds}), q-axis current command (i_{qs}^*), q-axis current (i_{qs}) and output

voltage magnitude of the current controllers ($|v_{dq}^*|$), where $|v_{dq}^*| = \sqrt{(v_{ds}^*)^2 + (v_{qs}^*)^2}$ and v_{ds}^*, v_{qs}^* are the output voltage command of d- and q-axes PI current controllers, for a step change of speed command from 0 rpm to +1600 rpm. It is seen from Fig 2.6 that i_{ds} is always kept zero and i_{qs} equals to I_{sm} for applying the maximum available torque to speed up the response. Also, $|v_{dq}^*|$ is always less than V_{cm}, the peak value of the triangle carrier signal, and this represents that the required stator voltage is always under the voltage limit of the inverter. To show the operating limit of $i_{ds} = 0$ control strategy, the same experimental results are given except ω_r^* is a step from 0 rpm to +2200 rpm which is outside the constant torque limit range. As shown in Fig. 2.7, the ω_r can not reach +2200rpm since $|v_{dq}^*|$ is equal to V_{cm} and no extra voltage can be applied to reduce the error between i_{qs}^* and i_{qs}. For comparison, the same experimental results as Fig. 2.7 except with weakening control strategy (negative i_{ds}) are be shown in Fig. 2.8. From the observation to Fig. 2.8, one can see that the ω_r can reach +2200rpm and the speed operating range can be effectively extended by field weakening control strategy.

Second, to demonstrate the classification of ten operating regions for four-quadrant operation, Fig. 2.9 shows the responses of ω_r^*, ω_r, i_{ds}, i_{qs}, $I_{qs\max}$ and $I_{qs\min}$ for a periodic step change of speed command from -2400 rpm to +2400 rpm and then back to -2400 rpm. Each speed command is fixed for 1.5 sec. It is seen from Fig. 2.9 that, for positive ω_r portion, speed ω_r at t_0, t_1, t_2, t_3, t_4 and t_5 correspond to 0, ω_{rm}, ω_{rc}, +2400 rpm, $\omega_{r\ n}$ and 0 rpm, respectively. Hence, according to the previous definition of operation regions, intervals (t_0, t_1), (t_1, t_2), (t_2, t_3), (t_3, t_4) and

(t_4, t_5) corresponds to the regions 1, 2, 3, 5 and 4, respectively. In fact, at t_1 the drive enters into the forward partial field weakening region (region 2) and enters to the forward full field weakening region (region 3) at t_2. Similarly, at t_3 and t_4, the drive enters into the forward weakening braking torque limit region (region 5) and the forward constant braking torque limit region (region 4). It is seen that, in spite of the abrupt and large torque change, the transitions are very smooth. Similarly, the other five regions for negative speed can also be observed from Fig. 2.9. The intervals (t_5, t_6), (t_6, t_7), (t_7, t_8), (t_9, t_{10}), (t_{10}, t_{11}) and (t_{11}, t_0) are corresponds to the regions 6, 7, 8, 8, 10 and 9, respectively. Moreover, one can see from Fig. 2.9 that, for example, for $t \in [t_2, t_4]$, $I_{qs\max}$ and $I_{qs\min}$ are no longer with equal magnitude due to considering the stator resistance. In fact, for $\omega_r \geq 0$ the maximum forward torque is limited by $I_{qs\max}$ and the maximum braking torque is limited by $I_{qs\min}$; On the contrary, for $\omega_r < 0$ the maximum forward torque is limited by $I_{qs\min}$ and the maximum braking torque is limited by $I_{qs\max}$.

Third, consider other experiments for illustrating the degraded performance resulting from the neglect of stator resistance, namely R_s is considered as zero. For consistency and comparison, the experimental set up of Figs. 2.10 and 2.11 are all the same except that the calculation of U/L I_{qs} bounds calculator of the former is based on the value shown in Table 2.1 and that of the latter is with the assumption of $R_s = 0$. As shown in the previous section, the most apparent difference between both is the maximum available braking torque. Therefore, the experiments with the same test conditions as that of Fig 2.9 is repeated twice. One is based on the values shown in Table 2.1 to compute the U/L I_{qs} bounds and the corresponding results are shown in

Fig 2.10. On the other hand, another experiment is with the assumption of $R_s = 0$ and the experimental results are shown in Fig. 2.11. The tested motor is operated in +2400 rpm at $t = 0$ and speed command step change from +2400 to -2400 rpm at $t = 0$. Comparing the braking time duration needed for the speed from +2400 to 0 rpm, one can find that the time duration of the results shown in Fig 2.10 is 252 ms and that of shown in Fig 2.11 is 275 ms. Therefore, the neglecting of stator resistor will result in a sluggish speed response.

From above experimental results, one can see that the $i_{ds} = 0$ control strategy can obtain satisfactory performance during the constant torque limit range. However, the field weakening control strategy must be adopted to effectively extend the operating range to non-constant torque limit range. Also, the real U/L I_{qs} bounds must be fed to adjust the saturation bounds of the adopted PI speed controller to reflect truly the maximum available accelerating/ decelerating torque ability. As a result, the drive can keep the high dynamic response for four-quadrant drive operation. In order to facilitate understanding the significance of the filed weakening control strategy, the tested SMPMSM whose parameters are shown in Table 2.1 are selected as example. Moreover, the corresponding V_{sm} and I_{sm} are chosen as 50 V and 2 A, respectively. Fig. 2.12 shows the corresponding maximum torque-speed characteristics. From Fig. 2.12 one can see that the speed range of field weakening control strategy can be extended to 125 % of that of $i_{ds} = 0$ control strategy.

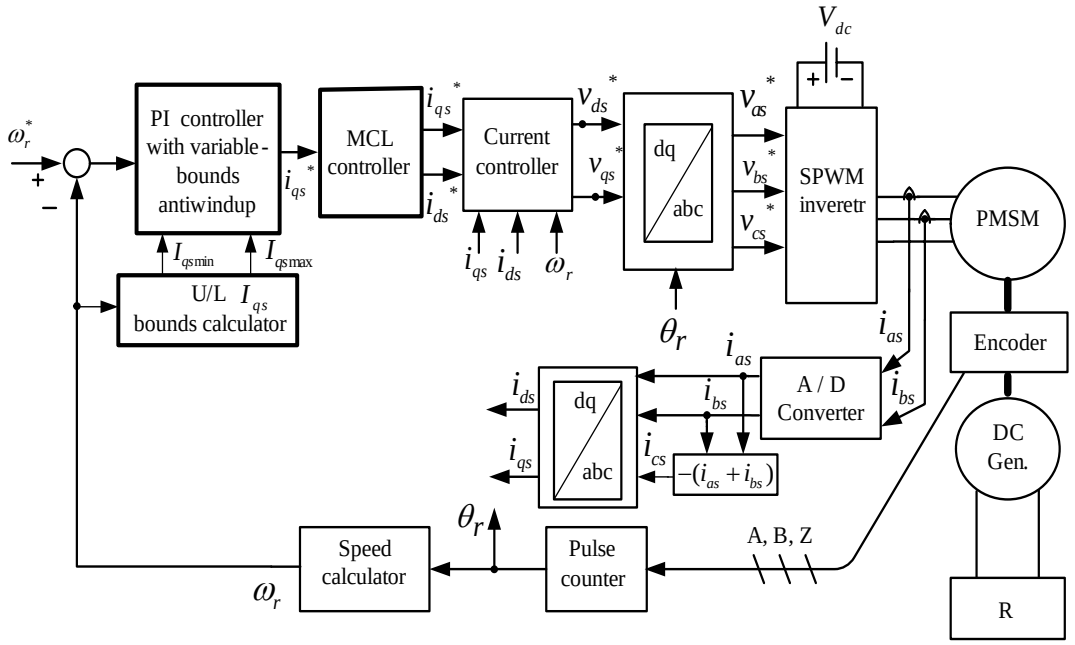

Fig. 2.4. Block diagram of the adopted speed control system for a SMPMSM drive.

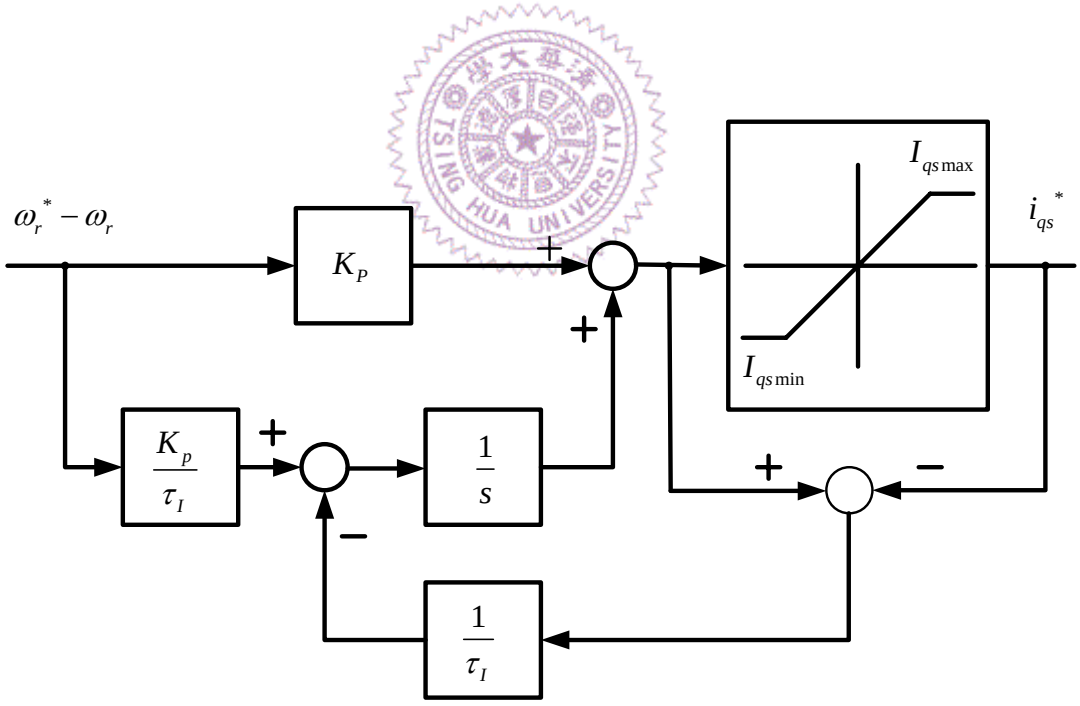

Fig. 2.5. Block diagram of the adopted PI speed controller with antiwindup [59].

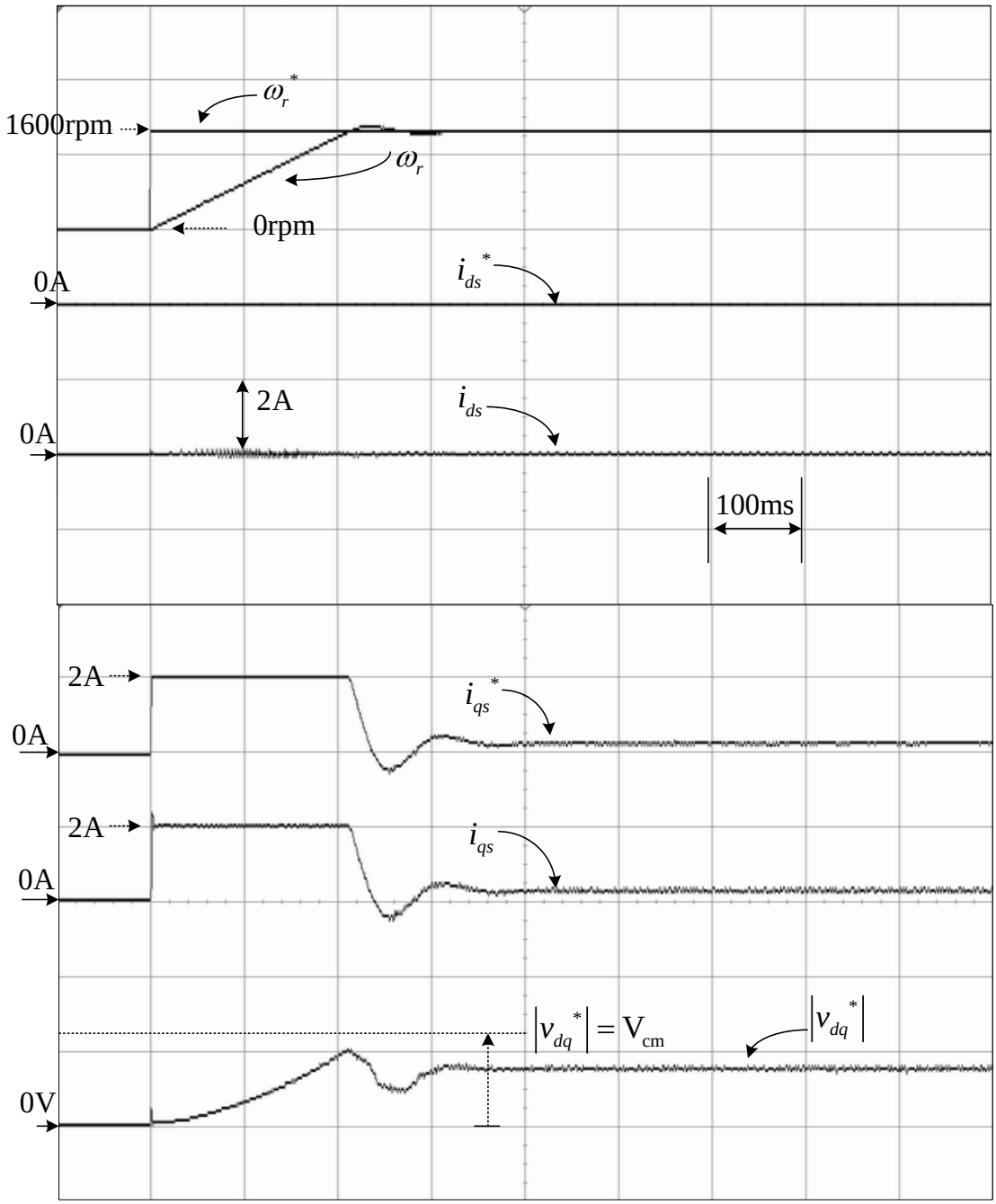

Fig. 2.6. Trajectories of ω_r^*, ω_r, i_{ds}^*, i_{ds}, i_{qs}^*, i_{qs} and $|v_{dq}^*|$, for a step speed command from 0 rpm to +1600 rpm and adopt $i_{ds} = 0$ control strategy.

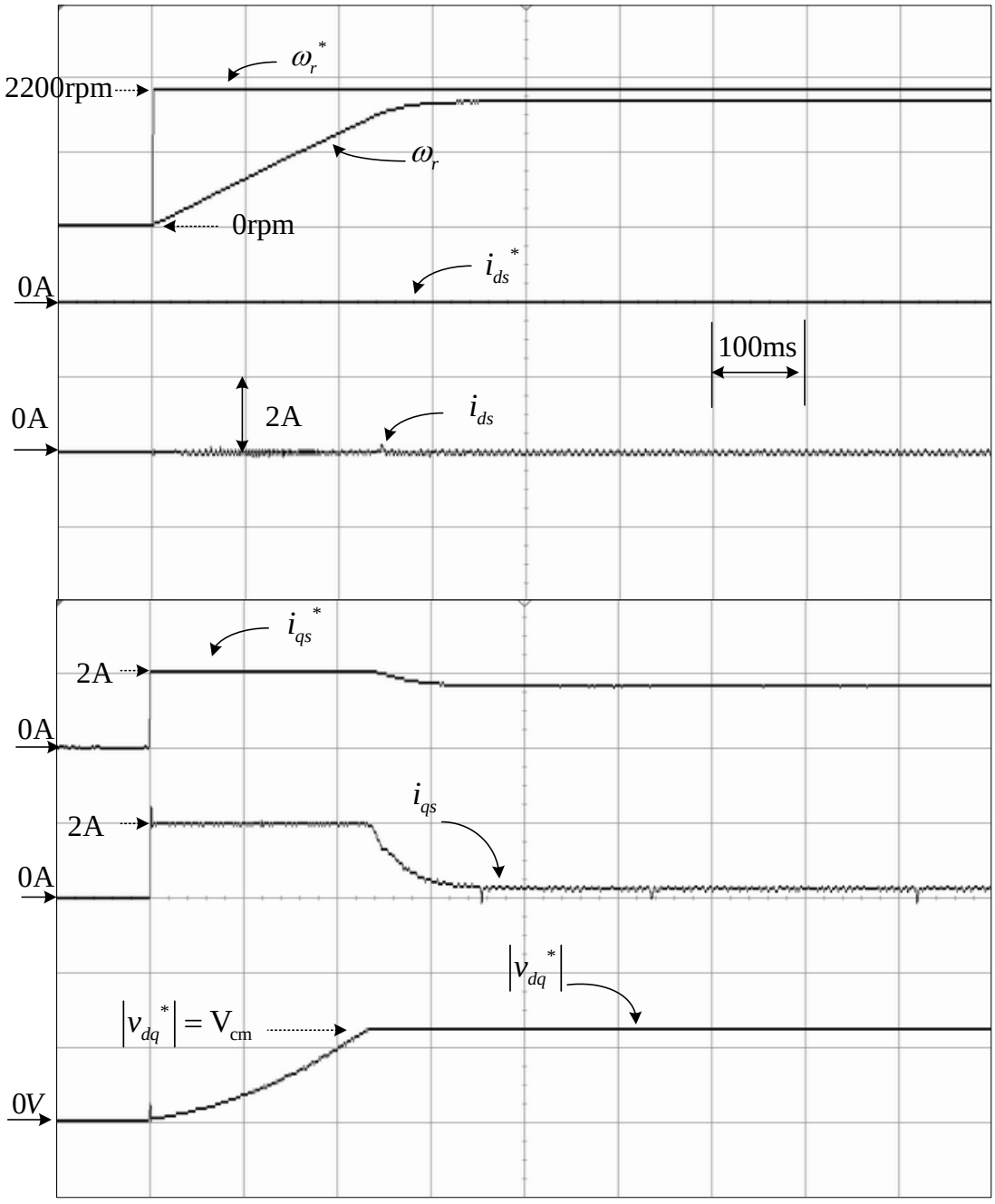

Fig. 2.7. Trajectories of ω_r^*, ω_r, i_{ds}^*, i_{ds}, i_{qs}^*, i_{qs} and $|v_{dq}^*|$, for a step speed command from 0 rpm to +2200 rpm and adopt $i_{ds} = 0$ control strategy.

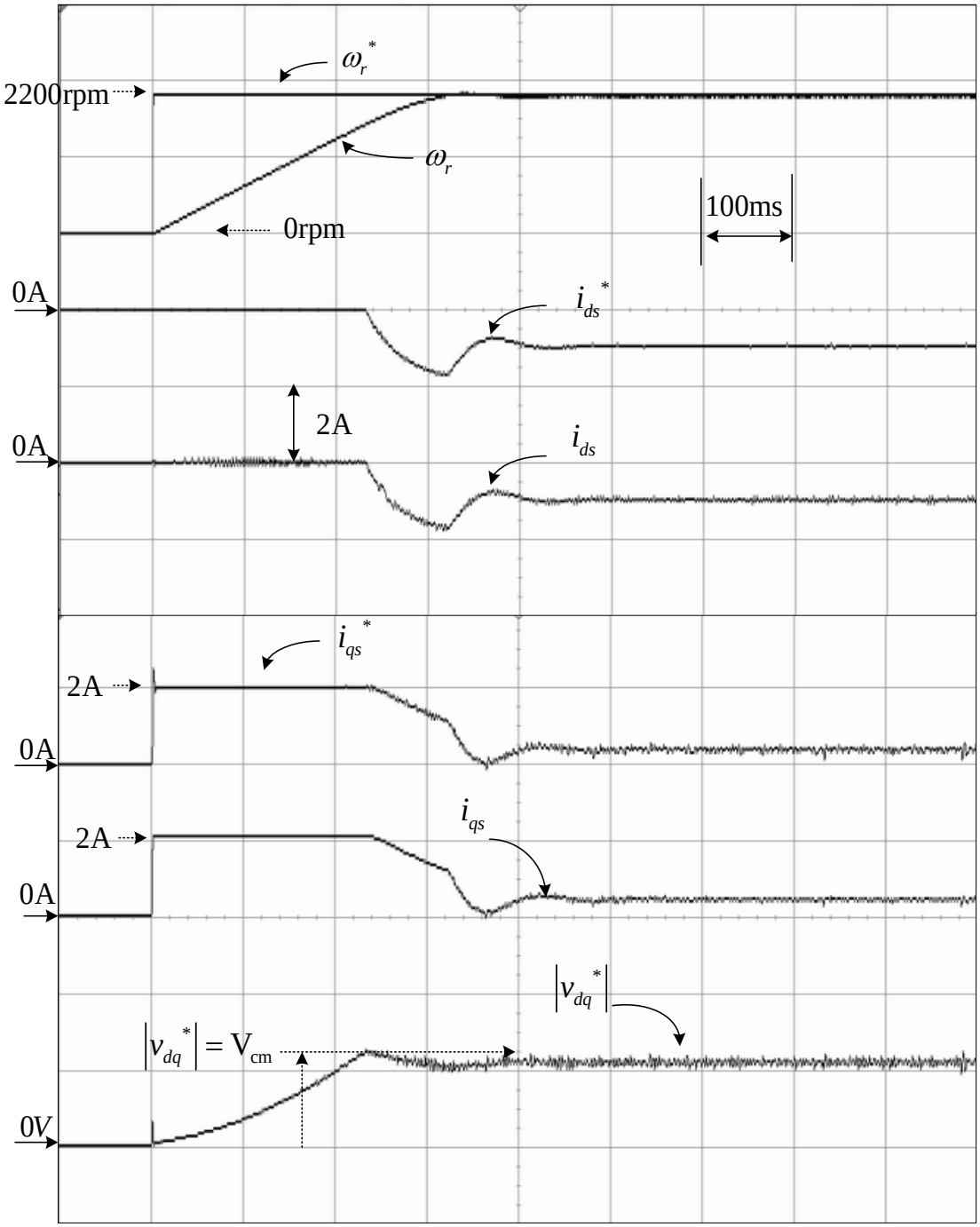

Fig. 2.8. Trajectories of ω_r^*, ω_r, i_{ds}^*, i_{ds}, i_{qs}^*, i_{qs} and $|v_{dq}^*|$, for a step speed command from 0 rpm to +2200 rpm and adopt field weakening control strategy.

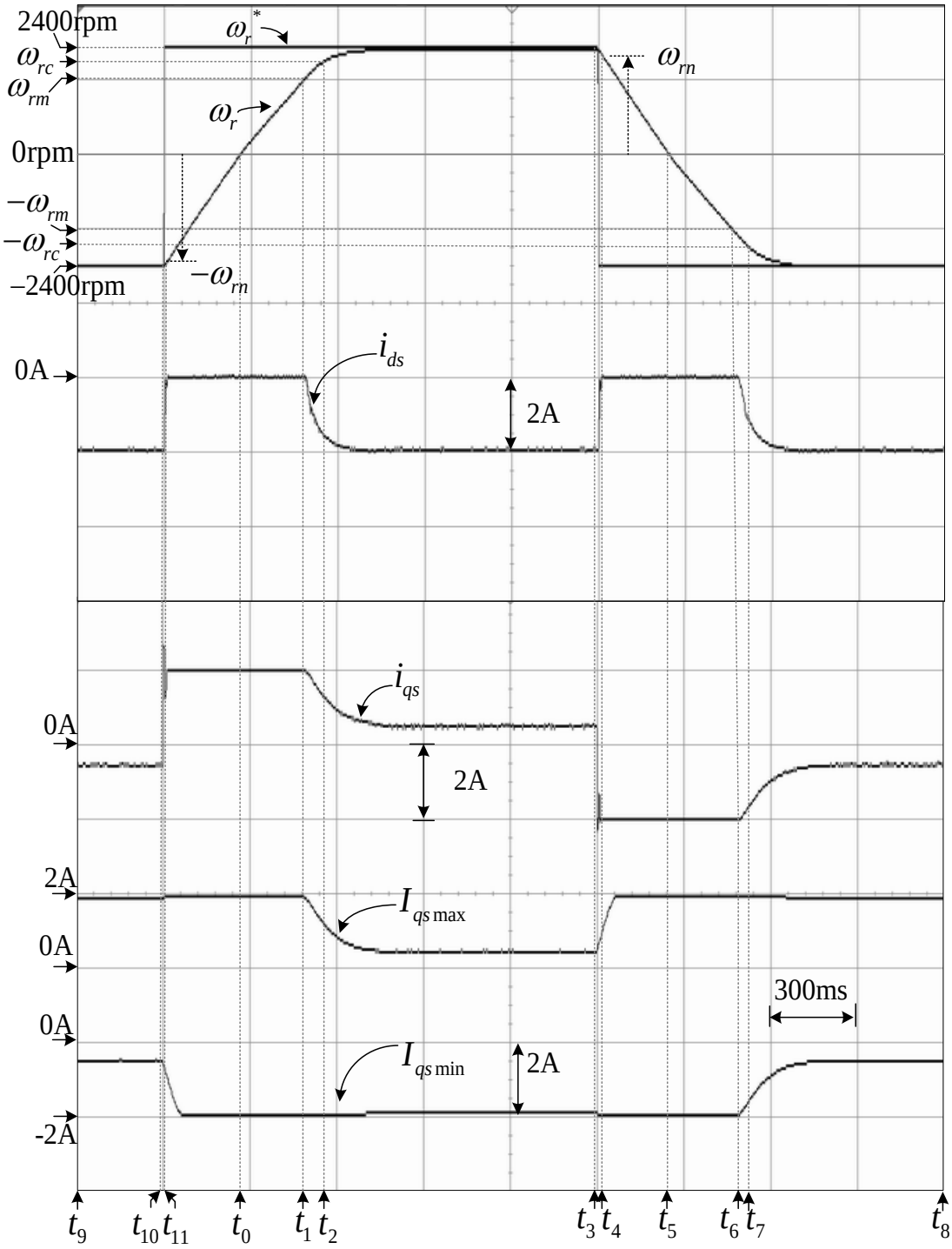

Fig. 2.9. Trajectories of ω_r^*, ω_r, i_{ds}, i_{qs}, $I_{qs\max}$ and $I_{qs\min}$, for a periodic step speed command from -2400 rpm to +2400 rpm.

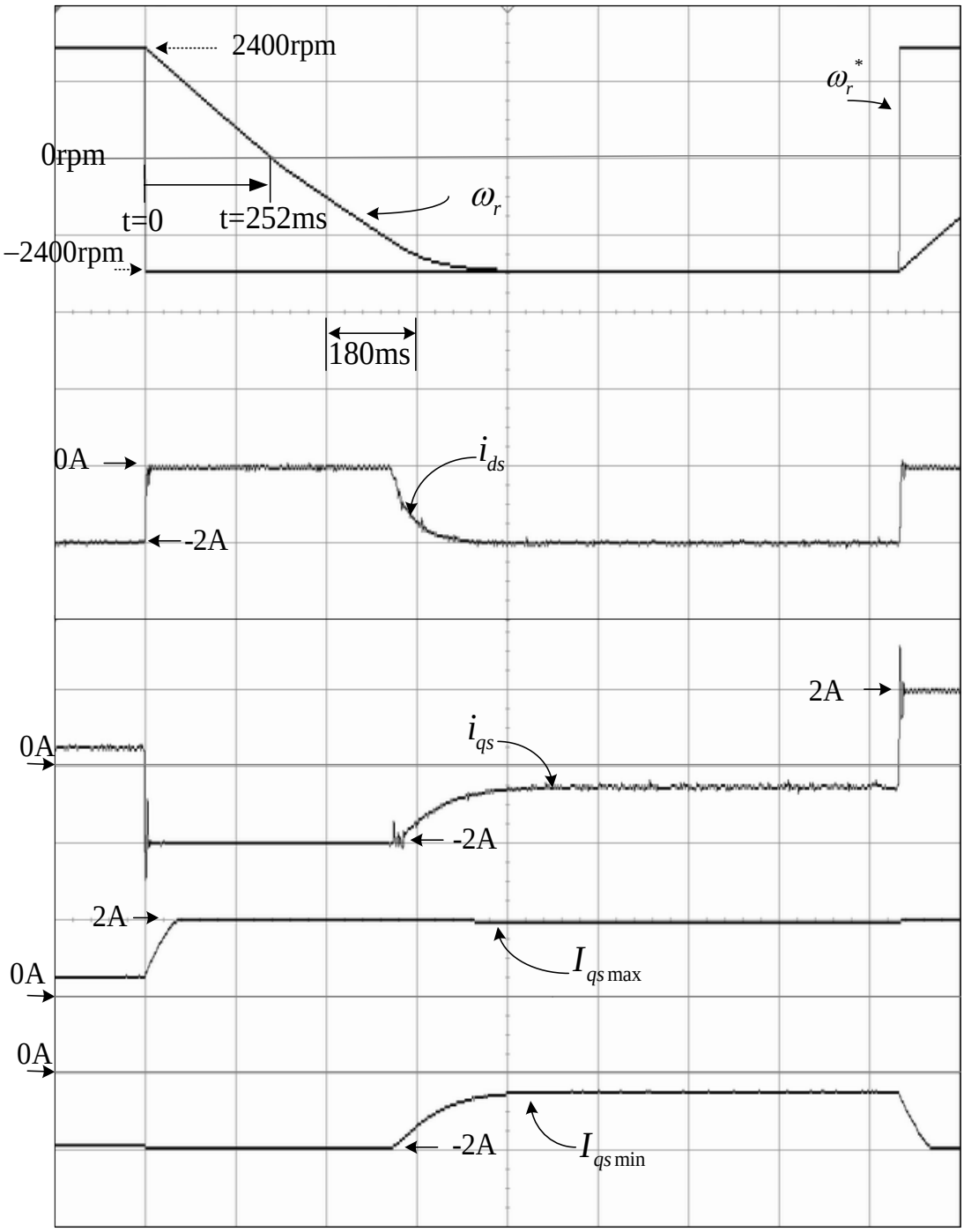

Fig. 2.10. Trajectories of ω_r^*, ω_r, i_{ds}, i_{qs}, $I_{qs\max}$ and $I_{qs\min}$, for a periodic step speed command from +2400 rpm to -2400 rpm and without neglecting R_s.

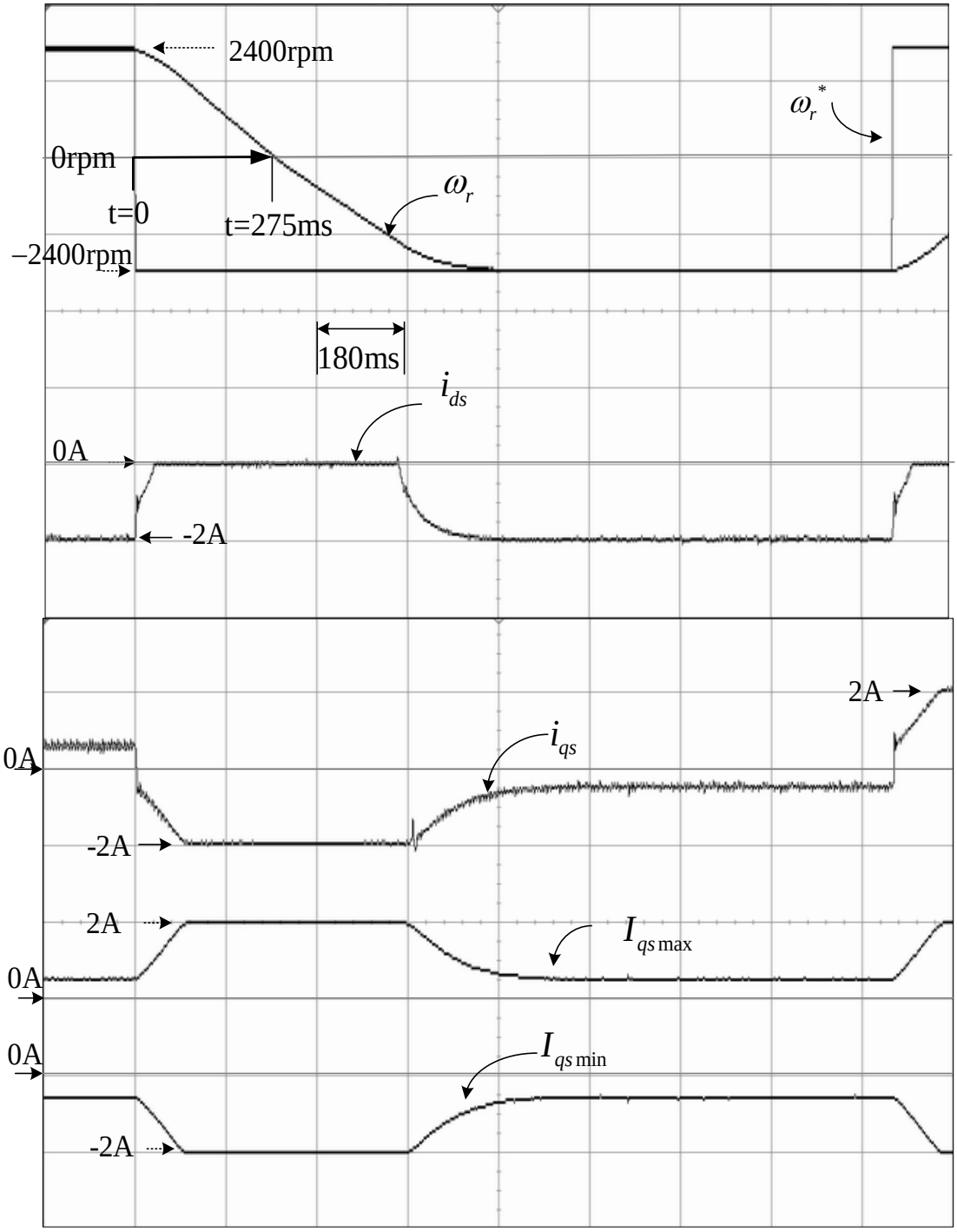

Fig. 2.11. Trajectories of ω_r^*, ω_r, i_{ds}, i_{qs}, $I_{qs\max}$ and $I_{qs\min}$, for a periodic step speed command from +2400 rpm to -2400 rpm and with neglecting R_s.

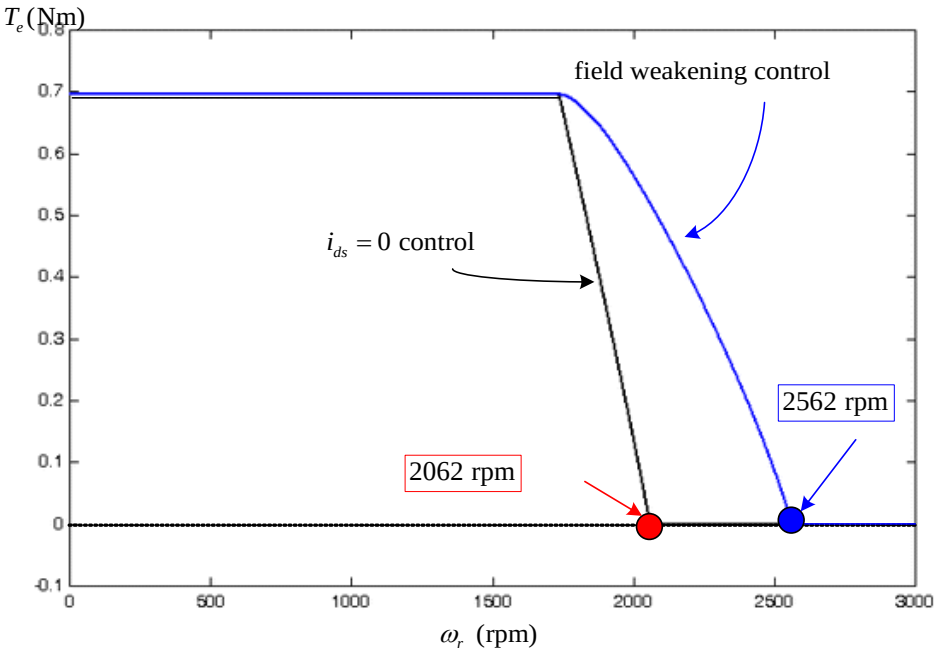

Fig. 2.12. The corresponding maximum torque-speed characteristics for $i_{ds} = 0$ and field weakening control strategy.